# BACH, the beamline for advanced dichroic and scattering experiments at ELETTRA

M. Zangrando[a] and M. Finazzi
*Laboratorio Technologie Avanzate, Superfici e Catalisi—Istituto Nazionale per la Fisica della Materia, c/o Sincrotrone Trieste, S.S. 14, Km 163.5 in Area Science Park, 34012 Basovizza–Trieste, Italy*

G. Paolucci, G. Comelli, B. Diviacco, R. P. Walker, and D. Cocco
*Sincrotrone Trieste, S.S. 14, Km 163.5 in Area Science Park, 34012 Basovizza–Trieste, Italy*

F. Parmigiani
*Istituto Nazionale per la Fisica della Materia and Dipartimento di Matematica e Fisica, Università Cattolica, Via Trieste 17, 25121 Brescia, Italy*

(Received 23 May 2000; accepted for publication 26 October 2000)

A beamline for advanced dichroism (BACH), to perform light polarization dependent experiments in the 35–1600 eV photon energy range is under construction at the ELETTRA Synchrotron Radiation Source in Trieste, Italy. The radiation source, based on two APPLE-II helical undulators, is designed for high photon flux and high resolving powers. The photons dispersion system is based on a Padmore variable angle spherical grating monochromator with a typical resolving power of 20 000–6000, 20 000–6000, and 15 000–5000 in the energy ranges 35–200 eV, 200–500 eV, and 500–1600 eV, respectively. Two separate branches after the monochromator allow setting two independent experimental chambers. The photon flux in the experimental chamber(s), calculated at the best resolutions achievable and with the aperture of the slits set at 10 $\mu$m, is expected to be above $10^{11}$ photons's with linearly or circularly polarized light. In addition, a fourth grating operates in the 400–1600 eV range to provide a higher flux, $10^{12}$ photons's with smaller resolving power (10 000–2000), allowing fluorescence and x-ray scattering experiments. The refocusing section(s), based on plane elliptical mirrors in a Kirkpatrick–Baez scheme, will provide on the sample, a nearly free-aberration spot(s), whose dimensions are expected to be $200\times10$ $\mu$m$^2$ (horizontal$\times$vertical). In the following, the general layout of the beamline is reported and the characteristics of the optical elements, as well as the optical performances (resolving powers and efficiencies of the monochromator, flux, and spot dimensions) are described in detail.  [DOI: 10.1063/1.1334626]

## I. INTRODUCTION

Third-generation synchrotron radiation sources exhibit a photon flux several orders of magnitude larger with simultaneous better beam collimation and degree of polarization with respect to the older sources. Recent progress in insertion device technology has also led to the development of UV and x-ray sources able to provide polarization tunability. The efficient use of such sources has required a significant evolution of beam transport, focusing optics, and monochromator behavior. Hereafter, we present the characteristics of a beamline for advanced dichroism (BACH) under construction at ELETTRA (the synchrotron radiation facility in Trieste, Italy). BACH has been designed to deliver a high-intensity and high-brilliance flux of photons in the soft x-rays energy range (35–1600 eV) with full tunability of the light polarization. The purpose of this project is to perform light polarization-dependent electron and photon spectroscopies.

The demand from the scientific community for high-resolution and high-brilliance x-rays at third-generation facilities has been growing very fast in the last years. In particular, the beamlines offering light polarization tunability are among the mostly requested ones. The interest in the use of polarized light comes from the fact that excitations induced in condensed and soft matter by the absorption of a photon are affected by the polarization of the light by selection rules depending on the angular degrees of freedom of the ground and final states. In this case, information concerning the occupation number of exchange, crystal, or ligand field-split states or of Zeeman levels can be obtained. For this reason, light polarization-dependent spectroscopy has become a very powerful tool to study the electronic and magnetic properties of matter. These techniques have been applied to investigate the interplay between spin–orbit interaction, hybridization, exchange coupling, and crystal field in a variety of systems showing exotic behaviors such as oscillatory coupling in multilayers, perpendicular surface magnetic anisotropy, chirality, and giant magnetoresistance.[1] In the x-ray range, this information can be combined with the site and shell selectivity typical of core level spectroscopy. In this respect, one of the most successful techniques is magnetic circular dichroism in x-ray absorption, which depends on the first order polarization of the core hole, i.e., on the ground state, shell and site projected orbital, spin, and dipo-

[a]Electronic mail: marco.zangrando@elettra.trieste.it

 

lar moments.[2] Higher-order magnetic and nonmagnetic multipoles can be determined by studying the angular dependence and the spin of the electrons or the photons emitted in the decay of the core hole.[3]

Inelastic photon scattering experiments in the soft x-ray domain is a rather recent field of scientific research because of the very low cross sections involved and of the poor detection efficiency of spectrometers in this photon energy range. This topic has now attracted fast-growing attention thanks to high-brilliance third-generation synchrotron radiation facilities, where the photon flux must be maximized to the detriment of energy resolution to have significant counting rates. These techniques have been extensively applied to the investigation of core excited states and of the dynamics of decay processes in condensed matter.[4] With the help of circularly polarized light, they have also been employed to study element-specific moments as well as their energy distribution in the valence shell. The beamline optics has been designed to work either in a high brilliance mode, which is needed for scattering and fluorescence experiments, or with a highly monochromatic beam, necessary for absorption and photoemission measurements at high resolution. The possibility of switching between these two operating modes is offered by the beamline monochromator, where three gratings cover the whole accessible photon energy range with high resolving power, while a fourth grating, with a low groove density, covers the high-energy range with high efficiency. In the following paragraphs, we describe in details each component of the BACH beamline, giving relevant estimated optical characteristics such as resolving power, photon flux and density, higher order rejection rate, etc.

## II. SOURCE

The radiation source of BACH is a double APPLE-II undulator[5] producing on the axis of the electron orbit elliptically and linearly polarized light. The undulator for low energies (LE) has a period of 77.36 mm for 27 periods. The photon energy ranges from 22 to 300 eV using the first harmonic. The high energies undulator (HE), made by 44 periods of 48.36 mm length, produces radiation with energy between 185 and 700 eV in the first harmonic while higher energies are covered by higher harmonics (see Fig. 1).

The electron beam profile in a straight section of ELETTRA can be approximately described by a double gaussian with $\sigma_x \approx 240\,\mu$m and $\sigma_y \approx 43\,\mu$m ($E=2$ GeV, 10% coupling), with $x$ in the orbit plane and $y$ in the vertical one.[6] The sinusoidal oscillation widths in an insertion device are[7]

$$x_0 = \frac{K_y \lambda_0}{2\pi\gamma}, \quad y_0 = \frac{K_x \lambda_0}{2\pi\gamma}, \tag{1}$$

where $K_i$ are the deflection parameters and $\lambda_0$ is the undulator period. For the two undulators used by BACH, the greatest value of $K_y$ is 6.54 and the greatest value of $K_x$ is 4.70. Thus, electrons are deflected from the ideal orbit by amounts smaller than the electron beam dimensions. The maximum deflections are 18.3 $\mu$m in the plane of the electron orbit and 13 $\mu$m in the vertical one. As a consequence,

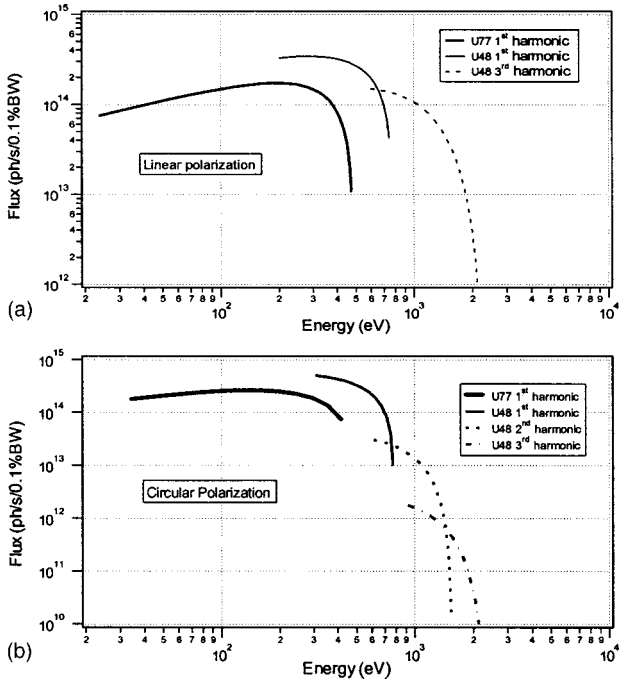


FIG. 1. Photon flux (Photons s/0.1% BW) out of the pinhole (defined angular divergence $=0.5\times0.1$ mrad$^2$) for the LE and HE undulators. The electron beam in the storage ring has an energy $E=2$ GeV and a current $I=100$ mA. (a) Linear polarized light; (b) circular polarized light.

$x_0$ and $y_0$ can be neglected. The size of the source then depends on $\sigma_x$ and $\sigma_y$ with a correction factor $\sigma_R$, which is a function of the wavelength $\lambda$ of the emitted photons and on the undulator length $L$. The dimensions of the source can be written as

$$\Sigma_x = \sqrt{\sigma_x^2 + \sigma_R^2}, \quad \Sigma_y = \sqrt{\sigma_y^2 + \sigma_R^2}, \tag{2}$$

where

$$\sigma_R^2 = 0.15\sqrt{\lambda L}. \tag{3}$$

Considering these corrections, the effective source dimensions are $\Sigma_x = 240\,\mu$m and $\Sigma_y = 50\,\mu$m, which are used in the present simulations. The angular divergence of the photon beam is determined by a pinhole between the source and the first mirror: its value is $0.5\times0.1$ mrad$^2$ (horizontal$\times$vertical).

The beamline is planned to perform light polarization dependent experiments in the energy range 35–1600 eV due to the choice of the two APPLE-II undulators as insertion devices,[5] capable of providing full tunability of the polarization of the light from linear to circular. The flux of these undulators, out of the $5\times1$ mm$^2$ pinhole put 10 m after the center of them, is presented in Fig. 1 for both polarizations. It can be seen that operations up to 1600 eV require the use of no higher than the third harmonic with the 48 cm undulator HE, while 35 eV can be reached with LE still in helical mode. Lower energies are still possible but only with linear polarization. It can also be seen that the overlap between the

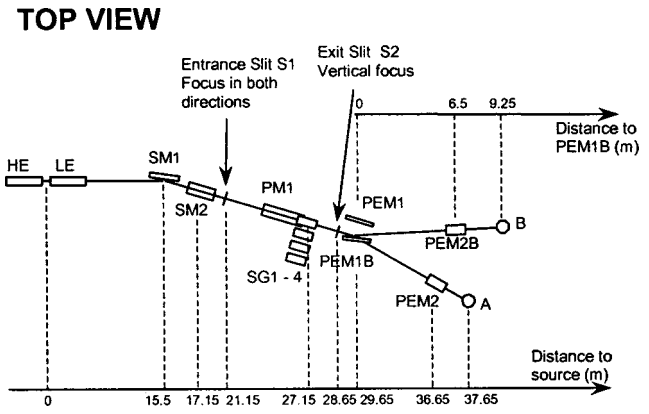


FIG. 2. Top view of BACH. HE and LE are the high and low energy undulators, respectively. SM1 and SM2 are the horizontal and vertical prefocusing mirrors. PM1 is the plane mirror of the monochromator, while SG1–4 is the set of four interchangeable gratings. PEM1 and PEM1B are the horizontal and vertical postfocusing mirrors and are used alternatively to direct the photon beam in the experimental chambers A or B. PEM2 and PEM2B are the vertical postfocusing mirrors.

energy spectra of the two devices is so good that it will not be necessary to use higher than the first harmonic for LE.

Another requirement for this beamline is the possibility of tuning the monochromator energy without changing the undulator gap. Two solutions have been developed: a small tapering of the gap itself and the use of even harmonics. Calculations shows that it is practical to have a tunability of at least 10% of the chosen energy over the entire photon energy range, when optimized for circular polarization. Similar results are expected in the linear, or any intermediate, polarization state. At low photon energies, up to 500 eV, the linewidth of the first harmonic is about 10% of the energy used. A gap tapering of 2 mm is capable of broadening the first harmonic up to ≈20% of the energy selected, maintaining 100% of circular polarization. The maximum reduction of the monochromatic photon flux occurs at 35 eV; in this case it is about one half of the flux without tapering. At higher energies it is necessary to use a higher harmonic which reduces both the linewidth and the degree of polarization. The tapering causes the spectrum to be very jagged and a better solution appears to be the use of an even harmonic that also results in a similar, or even higher, degree of polarization. This choice provides linewidths of 30%, instead of 2.5%, for 800 eV and 10%, instead of 1%, for 1400 eV of the photon energy selected with a degree of circular polarization about 90%. For the same photon energy, the flux of an even harmonic is about one third of the maximum value available with an odd harmonic.

## III. LAYOUT

### A. Beamline description

A general layout of the beamline is presented in Fig. 2. It consists of four sections: prefocusing section, monochromator, refocusing sections and experimental chambers. The prefocusing section includes a Kirkpatrick–Baez system of focusing[8] with two spherical mirrors SM1 and SM2. Both mirrors focus the radiation on the monochromator entrance slit plane. The monochromator is based on the original Padmore design[9] and includes a plane mirror PM1 and a set of interchangeable spherical gratings (SG1–4) that provide the vertical refocusing at the exit slit plane. To properly align both photon and electron spectrometer with the photon spot on the sample, the refocusing section(s) hosts a couple of plane elliptical mirrors mounted in Kirkpatrick–Baez configuration.[8] This permits us to independently move the spot on the sample in a vertical or horizontal direction without affecting the focusing of the spot, itself.

TABLE I. Optical characteristics of prefocusing elements of the sections.

| Mirror | SM1 | SM2 |
|---|---|---|
| Blank dimensions (mm×mm) | 330×40 | 160×30 |
| Blank height (mm) | 36 | 20 |
| Active area (mm×mm) | 300×5 | 100×10 |
| Blank material | Glidcop | Si |
| Coating material | Au | Au |
| Cooling | Internal | Lateral |
| Coating thickness (Å) | 300 | 300 |
| Radius of curvature (m) | 265.9 | 371.1 |
| Grazing incidence angle (°) | 1.75 | 1 |
| Tang. slope error rms (arcsec) | 0.5 | 0.1 |
| Sagittal slope error rms (arcsec) | 5 | 5 |
| Roughness rms (Å) | <5 | <5 |

### B. Prefocusing section

The prefocusing section is based on a Kirkpatrick–Baez system[8] made of two spherical mirrors. The main advantage of this kind of configuration is the complete decoupling between the horizontal and the vertical focusing, leading to an easier and more precise alignment of these two optical elements. These features are enhanced by the choice of spherical surfaces for the two mirrors whose characteristics are reported in Table I. The first mirror (SM1) is placed 15.5 m from the geometrical center of the straight section and it deflects the radiation horizontally. The second mirror (SM2), located 1.65 m after SM1, deflects the beam vertically. Both of these optical elements focus the radiation onto the entrance slit of the monochromator which is approximately 4 m behind SM2. Being the radiation source based on two different undulators, the images of these two mirrors will be different, too. In particular, a distance $\Delta$ between the sources will become a distance $\delta$ between the images with $\Delta/\delta$ proportional to the square of the demagnification factor, i.e.,

$$-\frac{\Delta}{\delta}\approx D^2. \tag{4}$$

Since the mean demagnification ranges from 15.5 to 5.65 ($D=2.8$) horizontally and from 17.15 to 4 ($D=4.3$) vertically, the distance between the foci of the different undulators, along the optical axis of the beamline, is about 30 cm for the horizontal foci and 13 cm for the vertical ones. The difference in focus position, in the horizontal direction, is completely negligible after the refocusing section, while the difference in the vertical direction is compensated by slightly changing the working curve of the monochromator.

The maximum emitted power from the insertion devices is about 200 W when the LE undulator works at its maxi-

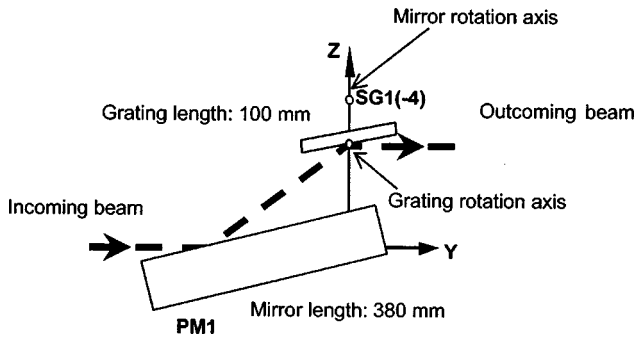


FIG. 3. Mechanical scheme of the variable included angle monochromator: the combined movement of PM1 (plane mirror) and one of the four spherical gratings SG1(−4) leads to the monochromatization of the light keeping both the entrance and exit slit fixed.

mum $K$ value ($E \approx 25$ eV).[10] Since this power impinges on SM1, this mirror undergoes to heavy thermal load (about 120 W). This thermal load causes the degradation of the optical surface quality that is strictly related to the focusing properties of the mirror. Since the plane of dispersion of the monochromator is vertical, SM1 focuses only horizontally to reduce the effects of the optical degradation on the flux and resolution of the light. To dissipate the energy absorbed by this mirror, a system for the internal cooling has been designed. The advantage of the present design over the more traditional lateral cooling arises from the proximity of the water circulating pipes to the optical surface (from 1 to 3 mm).

### C. Monochromator

The monochromator scheme follows the Padmore variable angle spherical grating monochromator (VASGM) design and is shown in Fig. 3. The incoming photon beam, focused onto the entrance slit in both directions (tangential and sagittal), impinges on the plane mirror PM1 (6 m after) and then is diffracted and focused tangentially (the first external order) by the spherical grating(s) SG1 (−4) onto the exit slit, 1.5 m downstream. In order to change the photon energy PM1 and SG1−4 must be rotated simultaneously (the mirror rotation axis is not coincident with the optical pole of PM1) using a variable included angle which permits us to keep fixed the tangential monochromatic focus onto the exit slit. This principle has been employed on the Petersen Plane grating monochromator (SX700)[11] and Padmore[9] has suggested it in a spherical grating monochromator. The choice of this type of monochromator has been motivated by the reliability already tested in other soft x-ray monochromators[12] and by the capability of high resolving powers in a broad range of energies.[12] This broad energy spectrum is covered by three gratings (SG1–3). The main difficulty with this design arises from the combined movements of PM1 and SG1−4 with the necessary precision. However, this problem is overcome by the present state of the mechanical manufacturing.[12,13]

With this design it is possible to maintain the beam direction and both slits fixed while the primary coma ($F_{300}$) is reduced considerably. Actually, as previously mentioned, the real source position depends on the energy range used. The displacement between LE and HE source positions is replicated at the entrance slit of the monochromator where there is the first focusing of the beam. Considering this fact, the entrance slit can be placed at two distinct positions corresponding to different tangential focal planes distant 12.7 cm. The difference in the distance between the slit and the grating, for a different energy range, is compensated by angular corrections on the gratings which permit us to always have a focused spot on the fixed exit slit without a loss of flux and/or resolution.

In Table II, the features of the optical elements of the monochromator are reported. All the gratings have laminar profiles assuring a good suppression of higher order light while keeping high resolution and efficiencies at various energy ranges; in particular SG1–3 cover 35–160 eV, 200–500 eV and 500–1600 eV ranges with estimated resolving powers of 20 000–6000, 20 000–6000, and 15 000–5000, respectively. The fourth grating SG4 provides a monochromatic beam in the 400–1600 eV range with resolving power smaller (10 000–2000) with respect to SG1–3 but allowing a greater flux. The estimated resolving powers have been calculated for different energies from 40 to 1600 eV. The conditions one has to satisfy are the grating equation ($F_{100} = 0$),[14] i.e.,:

TABLE II. Optical characteristics of the elements of a monochromator.

| Optical element | PM1 | SG1 | SG2 | SG3 | SG4 |
|---|---|---|---|---|---|
| Blank dimensions (mm×mm) | 410×60 | 100×30 | 100×30 | 100×30 | 100×30 |
| Blank height (mm) | 60 | 20 | 20 | 20 | 20 |
| Active area (mm×mm) | 380×10 | 80×10 | 80×10 | 80×10 | 80×10 |
| Blank material | Si | Si | Si | Si | Si |
| Coating material | Au | Au | Au | Au | Au |
| Cooling | Lateral | Lateral | Lateral | Lateral | Lateral |
| Coating thickness (Å) | 300 | 300 | 300 | 300 | 300 |
| Radius of curvature (m) | ∞ | 45 | 45 | 80 | 100 |
| Incidence angle (°) | Variable | Variable | Variable | Variable | Variable |
| Tang. slope error rms (arcsec) | 0.1 | 0.1 | 0.1 | 0.1 | 0.1 |
| Sagittal slope error rms (arcsec) | 5 | 5 | 5 | 5 | 5 |
| Roughness rms (Å) | <5 | <5 | <5 | <5 | <5 |
| Groove density (lines/mm) | ⋯ | 300 | 1200 | 1200 | 400 |
| Groove height (nm) | ⋯ | 45 | 11 | 7 | 10 |
| Groove width ($\mu$m) | ⋯ | 2.1 | 0.48 | 0.48 | 1.5 |

TABLE III. Optical characteristics of refocusing elements of the sections (branch A and branch B).

| Optical element | PEM1 | PEM2 | PEM1B | PEM2B |
|---|---|---|---|---|
| Blank dimensions (mm×mm) | 330×60 | 430×60 | 330×60 | 430×60 |
| Blank height (mm) | 40 | 40 | 40 | 40 |
| Active area (mm×mm) | 300×5 | 400×5 | 300×5 | 400×5 |
| Blank material | Fused silica | Fused silica | Fused silica | Fused silica |
| Coating material | Au | Au | Au | Au |
| Cooling | None | None | None | None |
| Coating thickness (°) | 300 | 300 | 300 | 300 |
| $r:r'$ | 800:850 | 800:100 | 800:975 | 750:275 |
| Grazing incidence angle (°) | 2.2 | 1 | 2.2 | 1 |
| Tang. slope error rms (arcsec) | 0.5 | 0.25 | 0.5 | 0.25 |
| Sagittal slope error rms (arcsec) | 5 | 5 | 5 | 5 |
| Roughness rms (°) | <5 | <5 | <5 | <5 |

$$\sin(\alpha)-\sin(\beta)=Nk\lambda, \tag{5}$$

where $\alpha$ and $\beta$ are the incidence and diffraction angle, respectively, $N$ is the groove density of the grating, $k$ is the order of diffraction, and λ wavelength of the diffracted radiation and the tangential focus condition $F_{200}=0$, i.e.,

$$\left(\frac{\cos^2\alpha}{r}-\frac{\cos\alpha}{R}\right)+\left(\frac{\cos^2\beta}{r'}-\frac{\cos\beta}{R}\right)=0. \tag{6}$$

The founded values of $\alpha$ and $\beta$ are used in the simulations to calculate the resolutions. In the estimation of the resolving power, the exit slit is kept open at 10 $\mu$m that is approximately the vertical dimension of the monochromatic image after the gratings. The results are presented in detail and discussed in the next section.

### D. Refocusing section

The first element of the refocusing section, 1 m after the exit slit of the monochromator, is a plane elliptical mirror PEM1 (PEM1B for branch B). Its reflecting surface is vertical, so it focuses the beam horizontally in the experimental chamber. The vertical refocusing is provided by a second plane elliptical mirror PEM2 (PEM2B for branch B) placed 7 m (6.5 m for B) downstream with the reflecting surface horizontal facing down. The characteristics of the optical elements of the refocusing section(s) are reported in Table III.

The separation between the two branches A and B is made feasible by keeping the two horizontally refocusing mirrors as close as possible to the exit slit in order to get the largest separation. The mirrors are interchangeable in a vacuum. A grazing angle of incidence of 2.2° guarantees enough room between the two branches and therefore the possibility to allocate the two vertical refocusing mirrors, followed by the two experimental chambers.

The vertical refocusing mirrors are kept as close as possible to the experimental chambers, in order to obtain vertical spots about 10–25 $\mu$m. The constrain given by the geometry of the Elettra experimental hall,[6] together with the necessity to leave enough room between the refocusing mirrors and the experimental chamber, allows a vertical demagnification of 8:1 for branch A and 7.5:2.75 for branch B. For x-ray scattering, the emitted photons must be detected versus their energy. To perform this measure, a photon spectrometer[15] must be used. The spot on the sample becomes the source of photons for the spectrometer. For this reason, the spot profile in the experimental chamber should be adapted to these experiments. In particular, to exploit the performances of the spectrometer, the vertical dimension of the spot should be less than 10 $\mu$m, while the horizontal size does not have any constrain. A plane elliptical surface for the refocusing mirrors responds to these requirements. These surfaces can only be manufactured with larger slope errors (about 0.3 in. root-mean-square (rms) vs 0.1 in. or even 0.05 in. rms) than spherical surfaces, tangentially. However, the nearly aberration-free spot shape compensates this limit (especially for large angular beam divergence as in our case). The ray tracing was performed using the SHADOW code.[16] For the refocusing stage, spherical mirrors (with tangential slope errors of 0.1 in. rms) were compared to plane elliptical mirrors with tangential slope errors of 0.5 in. rms and 0.25 in. rms for the horizontal and vertical directions, respectively. The results at energy of 200 eV for branches A and B are presented in Fig. 4. It can be seen that spherical aberrations heavily affect the spot shape leading to a spot size greater than the corresponding one for elliptical refocusing mirrors though the latter have a poorer optical quality. This result is obtained for all the energies of interest.

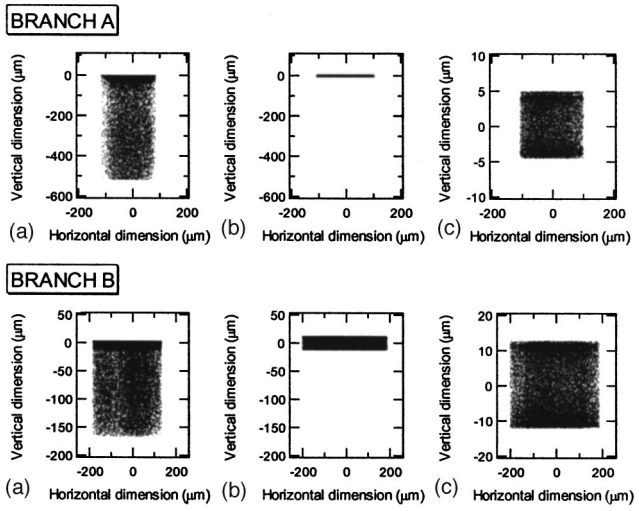


FIG. 4. Comparison among spots in the experimental chambers of the two branches (A and B) using (a) spherical and (b) plane elliptical mirrors in the refocusing section. (c) is equal to (b) but with different scale.

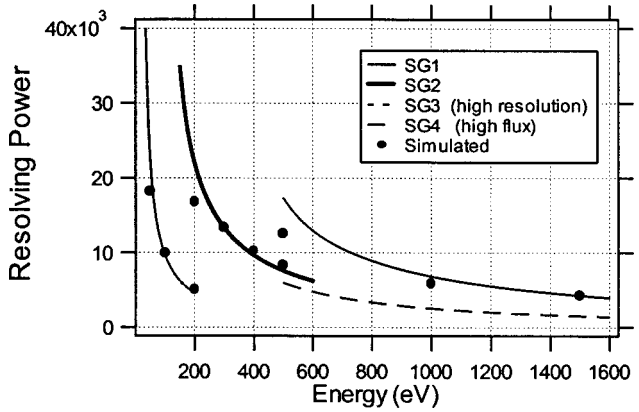


FIG. 5. Calculated resolving powers (lines) compared with simulated ones (dots). The resolving power is calculated taking into account the effects of the entrance and exit slit dimensions, the slope errors of the gratings and the residual aberrations (coma). The simulated resolving powers are obtained using the ray tracing program SHADOW and are referred to the real (measured) profiles of the gratings 1, 2, and 3 (i.e., the effect of the slope errors is included).

## IV. OPTICAL PERFORMANCES

### A. Resolution and gratings efficiency

An accurate estimation of the resolving power of a monochromator is obtained by taking into account the contributions, to the bandpass, $\Delta\lambda$, of different terms such as the entrance and exit slit dimensions, the slope errors, and the residual aberrations. Each of them contributes with a bandpass enlargement $(\Delta\lambda)_i$ and the final resolving power $\lambda/\Delta\lambda$ is the result of the convolution of the single terms $(\Delta\lambda)_i/\lambda$. In particular, these terms are[14]

$$\frac{(\Delta\lambda)_1}{\lambda} = \frac{1}{Nk}\frac{s}{r}\cos\alpha, \quad \text{entrance slit,} \tag{7}$$

$$\frac{(\Delta\lambda)_2}{\lambda} = \frac{1}{Nk}\frac{s'}{r'}\cos\beta, \quad \text{exit slit,} \tag{8}$$

$$\frac{(\Delta\lambda)_3}{\lambda} = \frac{2\sigma\cos\Theta}{Nk}, \quad \text{slope error,} \tag{9}$$

$$\frac{(\Delta\lambda)_4}{\lambda} = \frac{3}{2}\frac{1}{Nk}L^2F_{300}, \quad \text{coma,} \tag{10}$$

where $N$ is the groove density, $k$ the order of diffraction, $\alpha$ the incidence, and $\beta$ the diffraction angle, $s$ the entrance slit width, $s'$ the exit slit width, $r$ the distance between the entrance slit and the grating, $r'$ the distance between the grating and the exit slit, $\sigma$ the slope error of the grating, $\Theta$ the included angle $(\alpha+\beta)$, $L$ half of the dimension of the illuminated spot at the grating, and $F_{300}$ the coma aberration term. The estimated resolving power obtained taking into account all of these terms is represented in Fig. 5. These theoretical values should be compared with the resolving powers obtained from ray tracing simulations[16] at various energies. The latter are also present in Fig. 5 as single points. In the simulations all the effects, including the aberrations and the real measured profiles of the gratings and mirrors are taken into account. We can observe that ''simulated'' resolving power values are in good agreement with theoretical values. For SG1, the agreement is very good for energies between 100 and 200 eV, while for 50 eV the simulated resolving power is approximately two thirds of the ideal value. This behavior is almost the same for SG2 and SG3. The difference at lower energy is typically due to the residual aberrations. Their contribution increases with decreasing energy for this design and, at higher resolving power, every small deviation from the ideal configuration reduces the performances.

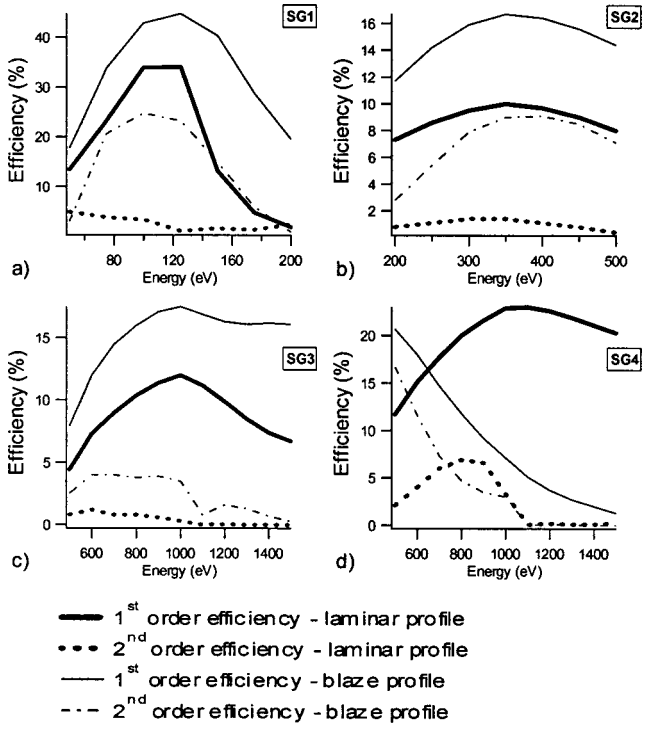


FIG. 6. Comparison between efficiencies of laminar and blaze gratings for different groove densities. Thicker curves refer to the laminar profile: the solid curves represent first order efficiencies and the dotted ones represent second order efficiencies. Thinner curves refer to the blaze profile: the solid curves represent first order efficiencies and the dot line ones represent second order efficiencies. (a) SG1→300 l/mm, $R_{\text{curvature}}$=45 m; (b) SG2→1200 l/mm, $R_{\text{curvature}}$=45 m; (c) SG3→1200 l/mm, $R_{\text{curvature}}$=80 m; (d) SG4→400 l/mm, $R_{\text{curvature}}$=100 m.

Another important feature of the gratings is their efficiencies at every energy of interest. Calculating both the efficiency for blaze or laminar profile,[17] for the first and second external order of diffraction, some evident results appear (see Fig. 6). The first conclusion is that blaze gratings offer absolute efficiencies that are always greater than the corresponding values for laminar gratings. The only exception is represented by the grating SG4, where the small grazing angle of incidence would require blaze angle lower than 1°, almost impossible to be realized. The advantage of laminar over blaze profiles is clearly seen for the relative efficiencies (first over second diffraction order efficiency). These quantities are larger for the laminar case as shown in Fig. 7. It means that the laminar profile is more efficient to reduce the unwanted monochromator secondary orders. Therefore, laminar profiles, as the best compromise between absolute and relative efficiency, are chosen.

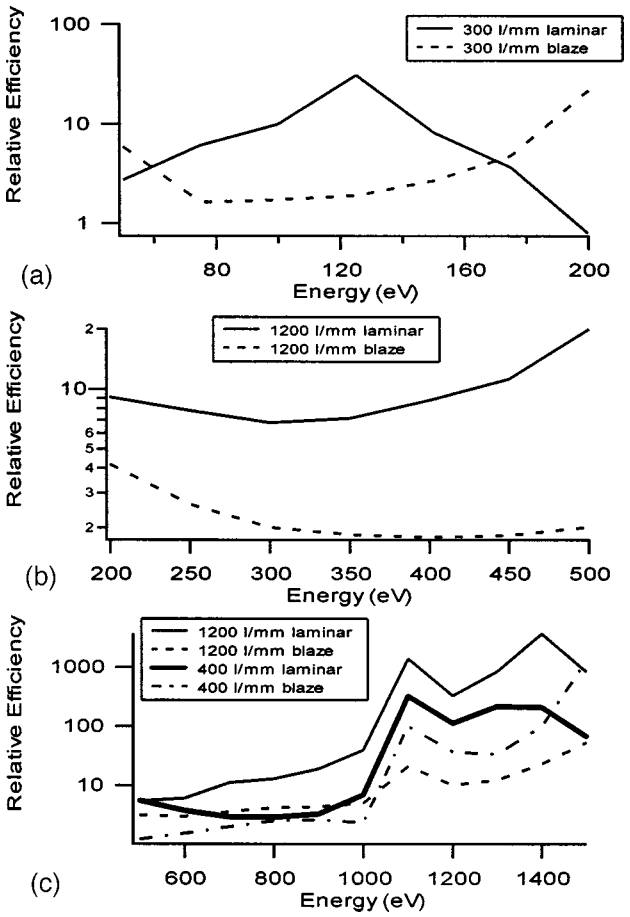


FIG. 7. Relative efficiencies (first/second order) of the four gratings used in BACH's monochromator: (a) SG1; (b) SG2; (c) SG3; and SG4.

### B. Flux

One of the main features of BACH is the possibility to perform fluorescence and x-ray scattering measurements in the soft x-ray region. For these experiments, the number of photons impinging on the sample is a determining factor whereas the resolving power can be slightly degraded. The simulation of the flux of the undulators at the pinhole output, performed using the URGENT code[10] is reported in Fig. 1. Considering the grating efficiency, the mirrors reflectivity, and including the geometrical losses, the expected photon fluxes in the experimental chambers are reported in Table IV. The flux is calculated at maximum resolving power, and is distributed on a $10\times200\,\mu m^2$ spot for branch A and on a $25\times300\,\mu m^2$ spot for branch B.

TABLE IV. Photon flux in experimental chambers for each of the four spherical gratings; for every energy the flux is calculated at the maximum resolving power achievable with entrance and exit slit width set to 10 $\mu$m.

| SG1 | | SG2 | |
|---|---|---|---|
| $E$ (eV) | Flux ($10^{11}$ Ph/s) | $E$ (eV) | Flux ($10^{11}$ Ph/s) |
| 50 | 3.97 | 200 | 1.98 |
| 75 | 14.65 | 250 | 1.83 |
| 100 | 36.92 | 300 | 2.28 |
| 125 | 52.14 | 350 | 2.64 |
| 150 | 23.30 | 400 | 2.86 |
| 175 | 7.22 | 450 | 2.70 |
| 200 | 1.79 | 500 | 2.18 |
| SG3 | | SG4 | |
| $E$ (eV) | Flux ($10^{11}$ Ph/s) | $E$ (eV) | Flux ($10^{11}$ Ph/s) |
| 600 | 0.84 | 600 | 5.19 |
| 700 | 1.21 | 700 | 7.15 |
| 800 | 1.50 | 800 | 8.71 |
| 900 | 1.71 | 900 | 9.83 |
| 1000 | 1.74 | 1000 | 11.62 |
| 1200 | 1.45 | 1200 | 11.73 |
| 1500 | 0.51 | 1500 | 6.53 |

## ACKNOWLEDGMENTS

The authors would like to thank Alessandro Gambitta, Claudio Fava, and Massimiliano Tudor (ELETTRA mechanical engineering group) for the assistance in the mechanical specification and design, Giovanni Sostero (ELETTRA soft x-ray and optical metrology laboratory) for the assistance in the measurements and characterizations of the optical surfaces, and the colleagues of ELETTRA and INFM for their help. This work is supported by the Istituto Nazionale per la Fisica della Materia, Progetto Luce di Sincrotrone BACH.

[1] See, for instance *Synchrotron Radiation and Magnetism*, edited by E. Beaurepaire, B. Carrière, and J. P. Kappler (Edition de Physique, Paris, 1997).
[2] P. Carra, B. T. Thole, M. Altarelli, and X. Wang, Phys. Rev. Lett. **70**, 694 (1993).
[3] G. van der Laan and B. T. Thole, Phys. Rev. B **52**, 15355 (1995); J. Phys.: Condens. Matter **7**, 9947 (1995).
[4] See, for instance, F. Gel'mukhanov and H. Ågren, Phys. Rep. **312**, 87 (1999).
[5] S. Sasaki, Nucl. Instrum. Methods Phys. Res. A **347**, 83 (1994).
[6] ELETTRA Conceptual Design Report, 1989.
[7] B. Diviacco (private communications).
[8] P. Kirkpatrick and A. V. Baez, J. Opt. Soc. Am. **38**, 766 (1948).
[9] H. A. Padmore, Rev. Sci. Instrum. **60**, 1608 (1989).
[10] URGENT, by R. P. Walker and B. Diviacco, Sincrotrone Trieste, Italy; XOP, by M. Sanchez del Rio and R. J. Dejus.
[11] H. Petersen, Opt. Commun. **40**, 402 (1982).
[12] W. B. Peatman, J. Bahrdt, F. Eggenstein, G. Reichardt, and F. Senf, Rev. Sci. Instrum. **66**, 2801 (1995).
[13] Bes Tec (private communications, 1999).
[14] W. Peatman, *Gratings, Mirrors and Slits* (Gordon and Breach, Amsterdam, 1997).
[15] D. Cocco, K. C. Prince, and M. Matteucci, Proc. SPIE **3450**, 17 (1998).
[16] B. Lai and F. Cerrina, Nucl. Instrum. Methods Phys. Res. A **246**, 337 (1986).
[17] LUMNAB, by M. Nevière, Centre National de la Recherche Scientifique, Marseille, France.